Journal of Hazardous Materials 186 (2011) 272–279

Contents lists available at ScienceDirect

Journal of Hazardous Materials

journal homepage: www.elsevier.com/locate/jhazmat

Porous $SnIn_4S_8$ microspheres in a new polymorph that promotes dyes degradation under visible light irradiation

Tingjiang Yan, Liping Li, Guangshe Li*, Yunjian Wang, Wanbiao Hu, Xiangfeng Guan

State Key Laboratory of Structural Chemistry, Fujian Institute of Research on the Structure of Matter, Graduate School of Chinese Academy of Sciences, Fuzhou 350002, People's Republic of China

ARTICLE INFO

Article history:
Received 17 July 2010
Received in revised form 28 October 2010
Accepted 29 October 2010
Available online 9 November 2010

Keywords:
Porous
$SnIn_4S_8$
Dyes
Degradation
Visible light

ABSTRACT

Porous $SnIn_4S_8$ microspheres were initially synthesized through a facile solvothermal approach and were investigated as visible-light driven photocatalysts for dyes degradation in polluted water. The photocatalysts were characterized by XRD, SEM, TEM, N_2 adsorption–desorption, and UV–vis diffuse reflectance techniques. Results demonstrated that the as-synthesized $SnIn_4S_8$ was of a new tetragonal polymorph, showing a band-gap of 2.5 eV, a specific surface area of 197 $m^2\ g^{-1}$, and an accessible porous structure as well. The photocatalytic activity of the porous $SnIn_4S_8$ was evaluated by decomposition of several typical organic dyes including methyl orange, rhodamine B, and methylene blue in aqueous solution under visible light irradiation. It is demonstrated that porous $SnIn_4S_8$ was highly photoactive and stable for dyes degradation, showing photocatalytic activity much higher than binary constituent sulfides like In_2S_3, SnS_2, or even ternary chalcogenide $ZnIn_2S_4$ photocatalyst. The excellent photocatalytic performance of porous $SnIn_4S_8$ is the consequence of its high surface area, well-defined porous texture, and large amount of hydroxyl radicals.

1. Introduction

Organic dyes are one of the largest pollutants released into wastewater from textile and other industrial processes, which have shown severe impacts on human physiology [1,2]. Some dyes like azo-dyes and fluorescein dyes have been found to be highly cytotoxic for the mammalian tissues [3,4]. The organic groups present in dyes result in the formation of certain reactive intermediates, which trigger the morphological and genetic alterations, thereby making the dye cytotoxic and carcinogenic. Recently, Inoue et al. [5] reported the carcinogenicity of anthraquinone dyes and found that the structure of the dye has an impact on the target organs. Therefore, disposal of the dyes from industrial wastewaters becomes a very relevant concern. Many approaches have been employed for the treatments of wastewaters containing dyes, which include the removal by biochemical processes [6], physical adsorption [7], electrocoagulation [8], ultracentrifugation [9], and wet air oxidation [10]. However, these approaches usually have low efficiency and cannot solve the post-disposal and regeneration problems.

Semiconductor photocatalysis, as a "green" technology, has been widely used to treat all kinds of contaminants, especially for the removal of organic contaminants [11–13]. It has many advantages over other treatment methods, such as environmental friendliness, ability to perform at ambient temperatures, and effectiveness to mineralize organic compounds at lower concentrations [14]. Among all photocatalytic materials previously reported, TiO_2 is popularly regarded as the photocatalysts for oxidative decomposition of organic compounds. Nevertheless, TiO_2 has a large band-gap of 3.2 eV and can only be excited by ultraviolet or near-ultraviolet radiation, which accounts for only about 4% of the solar light spectrum [15]. In order to efficiently utilize the solar light in visible region ($\lambda > 400$ nm) for decomposition of organic compounds, development of visible light driven photocatalysts has attracted a tremendous amount of attention. To date, modifying TiO_2 and developing new photocatalytic materials are two general strategies to extend the response of a photocatalyst to the visible light range [16]. Doping metals/nonmetals [17–21] and coupling with other lower band-gap semiconductors [22–24] have been utilized to enhance the photocatalytic activity under visible light irradiation. On the other hand, some single-phase oxides or sulfide photocatalysts, such as $BiVO_4$ [25], Bi_2WO_6 [26], $CaBi_2O_4$ [16], MIn_2O_4 (M = Ca, Sr and Ba) [27], CdS [28,29], ZnS [29], $CdIn_2S_4$ [30], and $ZnIn_2S_4$ [31] have been prepared, which have shown visible light driven photocatalytic activities for organic pollutant degradation. In contrast to the oxide photocatalysts, multi-component metal sulfides have narrower band-gap energies, which are promising to become a new class of visible light driven photocatalyst.

* Corresponding author. Tel.: +86 591 83702122; fax: +86 591 83702122.
E-mail address: guangshe@fjirsm.ac.cn (G. Li).

0304-3894/$ – see front matter © 2010 Elsevier B.V. All rights reserved.
doi:10.1016/j.jhazmat.2010.10.114

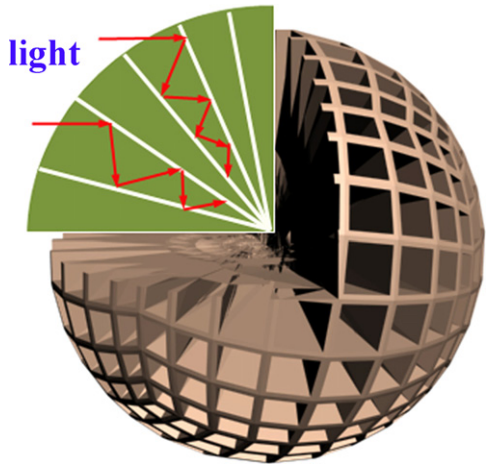

Scheme 1. Proposed model of light transfer paths, reflection, and scattering processes within the hierarchically porous structure.

Hierarchically porous materials are of considerable interest as potential photocatalysts due to their particular configuration [32]. As illustrated in Scheme 1, (1) the pores within the hierarchical structure can serve as the light-transfer paths for distribution of photon energy onto the inner surfaces of mesoporous frameworks, allowing light waves to penetrate deeply inside the photocatalyst and making it more efficient to work as a light harvester [33]; (2) taking into account the light absorption, reflection, and scattering within such a hierarchical porous systems, the effective light-activated surface area can be significantly enhanced, which would then improve the photoabsorption efficiency of the catalyst [34], and (3) hierarchical arrangement of macro- and meso-pores is important in reactants and product traffic control and in the resistance of the photocatalyst to poisoning by inert deposits [35]. Furthermore, these hierarchically porous materials possess large surface areas that can absorb more reactant molecules useful for degradation. Therefore, hierarchically porous structure in combination with the narrow band-gap may help to develop a general strategy for creating advanced photocatalytic properties in removal of organic dyes.

Stannum indium sulfide ($SnIn_4S_8$) is a typical ternary semiconductor chalcogenide that has a cubic spinel structure with the space symmetry group *Fd3m*, which shows many potential applications. For instance, the existence of vacancies in the spinel structure enables its uses in lithium insertion technology [36]. However, the photocatalytic activity for hierarchically porous $SnIn_4S_8$ is barely reported. In the present work, we reported on the synthesis of porous $SnIn_4S_8$ microspheres with a new tetragonal structure by a facial solvothermal method. The photocatalytic activities of the $SnIn_4S_8$ microspheres were initially studied for dyes degradation under visible light irradiation. Furthermore, possible reasons for the excellent activity of $SnIn_4S_8$ were discussed.

2. Experimental

2.1. Sample synthesis

All chemicals were of analytical grade and were used without further purification. In a typical procedure, 0.35 g of $SnCl_4{\cdot}5H_2O$ (1 mmol) and 1.173 g $InCl_3{\cdot}4H_2O$ (4 mmol) was dissolved in 80 ml of anhydrous ethanol in a flask under stirring at room temperature. When the solution became transparent, 0.76 g of thiourea (10 mmol) was introduced as a sulfur source. The mixture was stirred for about 30 min to become a transparent solution. Then, the above solution was sealed in a 100 ml Teflon-lined autoclave, which was heated in an electric desiccation box at 140 °C for 12 h and then cooled naturally to room temperature. The obtained precipitate at the jar bottom was collected, washed with distilled water and absolute ethanol several times, and finally dried in vacuum at 80 °C for 4 h.

Binary sulphides of In_2S_3 or SnS_2 were prepared according to the preparation procedure as mentioned above, while the corresponding metal chloride was used.

$ZnIn_2S_4$ photocatalyst was also prepared for comparison, which just followed the procedure previously reported in literature [31].

2.2. Sample characterization

Morphologies of the samples were observed by field emission scanning electron microscopy (FE-SEM) (JEOL JSM-6700). Chemical compositions of the samples were examined using energy-dispersive X-ray (EDX) analysis (JEOL JSM-6700). Microstructures of the samples were obtained by transmission electron microscopy (TEM) (JEM-2010), high-resolution TEM (HRTEM) (JEM-2010), and selected-area electron diffraction (SAED) pattern (JEM-2010). The crystal phases of the samples were examined by X-ray diffraction (XRD) using a Rigaku 2000 apparatus with Cu Kα irradiation. Lattice parameters of the samples were calculated by a least-squares method using Rietica Rietveld software. Raman spectra of the samples were recorded using a Perkin–Elmer Spectrum 2000 R NIR FT-Raman spectrophotometer, equipped with a Nd/YAG laser and a InGaAs detector. The contents of S, In, and Sn were determined using Ultima2 inductively coupled plasma (ICP) spectrometry and Vario MICRO elemental analyzer. X-ray photoelectron spectroscopy (XPS) analysis was conducted on an ESCALAB 250 photoelectron spectroscope (Thermo Fisher Scientific) at 3.0×10^{-10} mbar with monochromatic Al Kα radiation (E = 1486.2 eV). A Varian Cary 500 Scan UV/vis system was used to obtain the optical absorption spectra of the sample over a range of 200–800 nm.

Brunauer–Emmett–Teller (BET) surface areas and porosity of the sample were determined by nitrogen adsorption–desorption using a Mircromeritics ASAP 2000 surface area and porosimeter analyzer. The sample was degassed at 353 K overnight prior to BET measurement. The amount of hydroxyl radicals (•OH) produced during the photocatalytic reactions was detected in terms of a terephthalic acid (TA) photoluminescence (PL) probe method [37,38]. The visible light source and the cutoff filters were parallel to the photocatalytic reactivity test system. 40 mg of the final samples was added to an aqueous solution (80 mL) containing 10 mM NaOH and 5 mM TA in a 100 mL Pyrex glass vessel. At 20 min intervals, 3 mL aliquots were sampled and centrifuged to remove the catalysts. The •OH formed in the system react with TA and generate 2-hydroxyterephthalic acid (HTA), the fluorescence of which is directly proportional to the generated •OH. The fluorescence spectra were measured using an Edinburgh Analytical Instruments FL/FSTCSPC920 fluorescence spectrophotometer.

2.3. Photocatalytic activity measurement

Photocatalytic degradation of methyl orange (MO) was carried out in an aqueous solution at ambient temperature. The visible light source system consisted of a 300 W halogen lamp (Philips Electronics) and a composited cut-off filter that restricted the illumination in a range of 400–800 nm (as illustrated in inset of Fig. S1). Briefly, 15 mg of the samples was suspended in an 80 mL aqueous solutions containing 10 ppm of MO. The system was cooled by a fan and circulating water to maintain at room temperature. Prior to the irradiation, suspension was magnetically stirred in the dark to establish an adsorption–desorption equilibrium. A 3 mL aliquot was taken at 30 min intervals during the experiment and centrifuged to

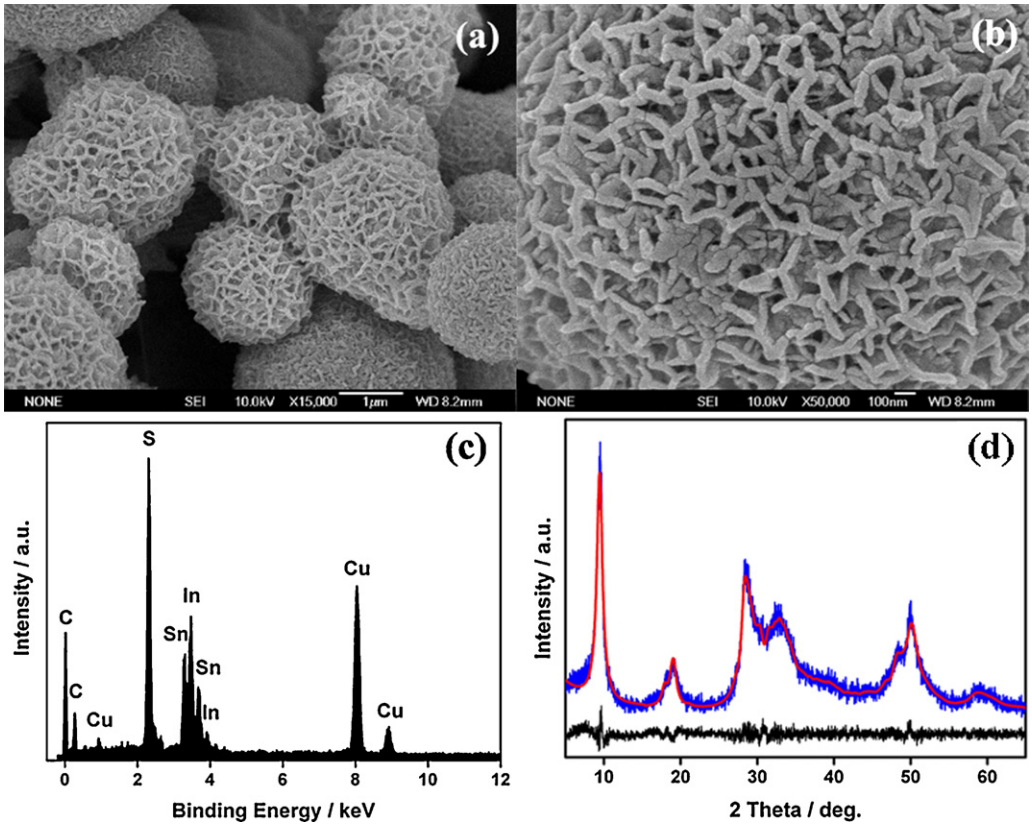

Fig. 1. (a) Low- and (b) high-magnification SEM images, (c) EDX spectrum, and (d) XRD patterns of the porous $SnIn_4S_8$ microspheres. Blue line denotes the experimental XRD data, red line represents the calculated XRD pattern, and black line is the difference spectrum.

remove the powders. The filtrates were analyzed on a Perkin-Elmer UV WinLab Lambda 35 spectrophotometer. The degradation percentage is reported as C/C_0, where C is the maximum peak of the absorption spectra of MO for each irradiated time interval at wavelength 464 nm and C_0 is the absorption intensity of the starting 10 ppm MO solutions. To test the stability, the sample was recycled and reused five times in the decomposition of MO under the same conditions. After each photocatalytic reaction, the aqueous solution was centrifuged to recycle the solids that were then dried at 353 K in vacuum for another test. In this stage, the concentration achieved at adsorption–desorption equilibrium was set as C_0. Rhodamine B (RhB) and methylene blue (MB) test conditions were the same to the MO test system, whereas the concentration of MB and RhB were 15 and 20 ppm, respectively. Total organic carbon (TOC) was measured with a Shimadzu TOC-4100 analyzer.

3. Results and discussion

3.1. Sample characterization

Fig. 1a shows the morphology of the sample in a large scale. It is indicated that the sample was composed of a large amount of nearly monodispersed network-like spheres with a diameter ranging from 2 to 4 μm. No other morphologies were detected, which indicates the formation of a high yield of 3D microspheres. An enlarged view of an individual sphere (Fig. 1b) indicates that the sample possessed a superstructure of a network-like appearance, which was constructed by numerous bending two-dimensional nanosheets with a thickness of about 40 nm. The aggregation and/or assembly of the nanosheets may produce abundant hierarchical pores at nanoscale.

Chemical compositions of these microspheres were examined using EDX analysis. As indicated in Fig. 1c, elements Sn, In, and S in addition to Cu and C arising from the copper grids were detected. The chemical compositions of the sample determined by ICP spectrometry showed that the formula for the microspheres agrees well with $SnIn_4S_8$, a compound which usually crystallizes in a cubic structure. Surprisingly, XRD pattern for the present $SnIn_4S_8$ did not match that for the cubic (Fig. 1d), since there appears one strong reflection at lower angle of about 9.5°. Careful structural refinements using Rietica program indicated that the porous $SnIn_4S_8$ microspheres possessed a tetragonal symmetry with lattice parameters of $a = 1.8915$ (±7) nm and $c = 1.0684$ (±5) nm. Three strong diffraction lines at two theta of 9.5°, 28.4°, and 50.0° were indexed in (2 0 0), (6 0 0), and (0 0 1) reflections, respectively. Reflection (2 0 0) was rather narrow, which indicates a large correlation length along this direction. In the refined XRD pattern (Fig. 1d), no other impurities such as binary sulfides, oxides, or metal-sulfur complex were detected. Different from the reported metal alkoxides with similar lamellar structures [39,40], this new tetragonal polymorph could be described as the stacked metal-sulfur sheets separated by bonded sulfide anions. More interestingly, when the sample was treated at 200 °C in N_2, this novel tetragonal structure could transform to the highly symmetric cubic structure as indicated by XRD (Fig. S2). This conclusion is also supported by comparing the Raman spectra of both polymorphs (Fig. S3).

Microstructures of the porous $SnIn_4S_8$ microspheres were further investigated by TEM and HRTEM. Fig. 2a displays a representative bright-field TEM image. The deep black TEM image indicates that the spheres were closely packed across the spherical centres. From the enlarged TEM image at the edge of one individual sphere (Fig. 2b), it is obvious that the colour of the spherical surface is light whereas the central part black. Therefore, the sphere surfaces were porous. These hierarchical microspheres were of polycrystalline nature, as confirmed by SAED pattern in Fig. 2c. A representative

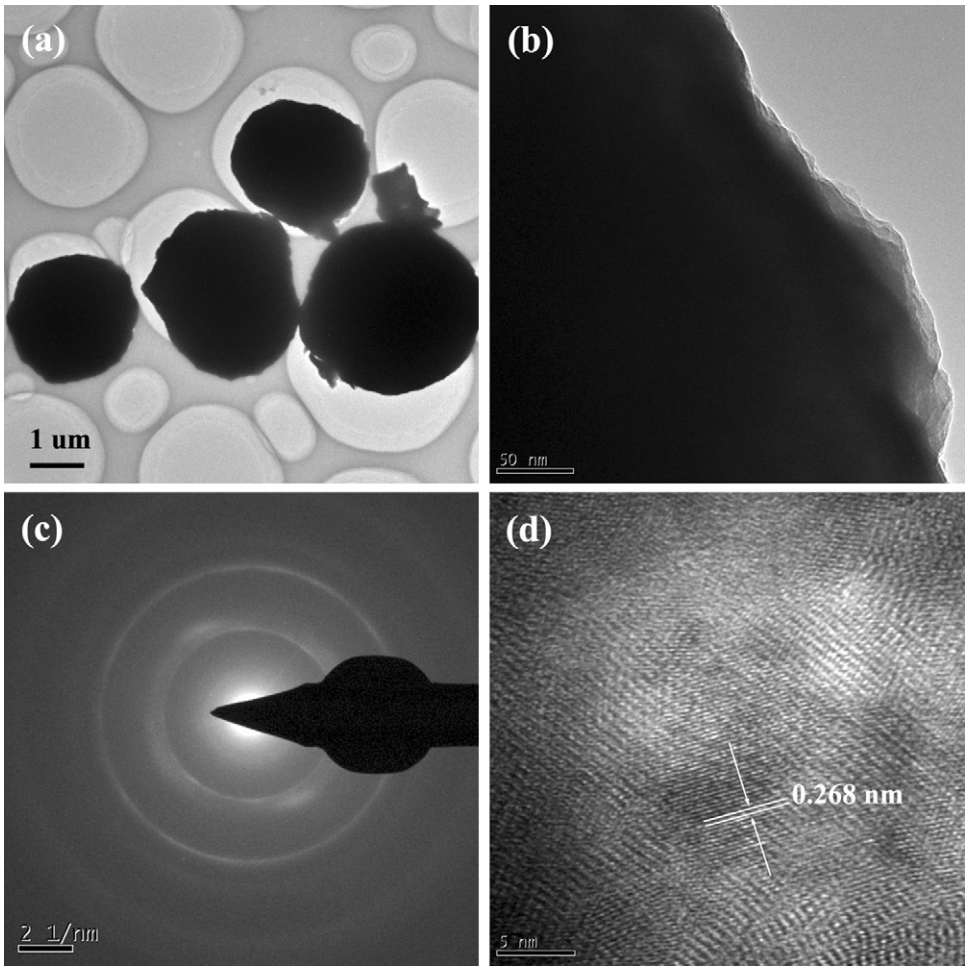

Fig. 2. (a) Low- and (b) high-magnification TEM images, (c) SAED pattern, and (d) high-resolution TEM image of the porous $SnIn_4S_8$ microspheres.

HRTEM image taken from the fringe part of a thin area is shown in Fig. 2d, which indicates a polycrystalline characteristic. The lattice fringes are clearly visible with a spacing of 0.268 nm. These microspheres also showed merits of extraordinarily high stability at ultrasonic conditions. Namely, these microspheres could sustain the hierarchical morphology intact when the ultrasonic time was prolonged from 5 to 30 min.

Porosity and surface area of the $SnIn_4S_8$ microspheres were investigated. Fig. 3 shows that the microspheres had a narrow pore size distribution, ranging from 2.0 to 5.0 nm, as calculated from desorption branch of a nitrogen isotherm by Barrett–Joyner–Halenda (BJH) method. Inset of Fig. 3 shows the corresponding nitrogen isotherm of the hierarchical $SnIn_4S_8$ spheres. According to the Brunauer–Deming–Deming–Teller (BDDT) classification, $SnIn_4S_8$ microspheres displayed a type-IV isotherm with a hysteresis loop in the range of 0.4–0.9P/P_0, implying the presence of mesopores [41,42]. BET surface area of the porous $SnIn_4S_8$ microspheres was about 197 $m^2\,g^{-1}$, much larger than those reported for Bi_2WO_6 (10 $m^2\,g^{-1}$) [43], ZnS (48 $m^2\,g^{-1}$) [44], and CeO_2 (92 $m^2\,g^{-1}$) [45] with similar morphologies. The increased surface area may be attributed to the small assembled hierarchical building blocks. Such type of hierarchical 3D architecture with a high surface area may be beneficial for applications as the catalysts for water treatments.

This hierarchical 3D architecture was first investigated for unique electronic states and optical properties necessary for property tailoring. Fig. 4 represents the UV–vis absorption spectrum of the porous $SnIn_4S_8$ microspheres. It is shown that the photoabsorption is distributed from UV light region to the visible light shorter than 550 nm, and that there existed an intense adsorption with a steep edge in the visible light region. Such a steep shape of the spectrum indicates that the visible light absorption band is not due to the transition from impurity levels but the band-gap transition. A classical Tauc approach is employed to estimate the band-gap energy E_g of the $SnIn_4S_8$ microspheres [46]. Plot of $(\alpha h\nu)^2$ against

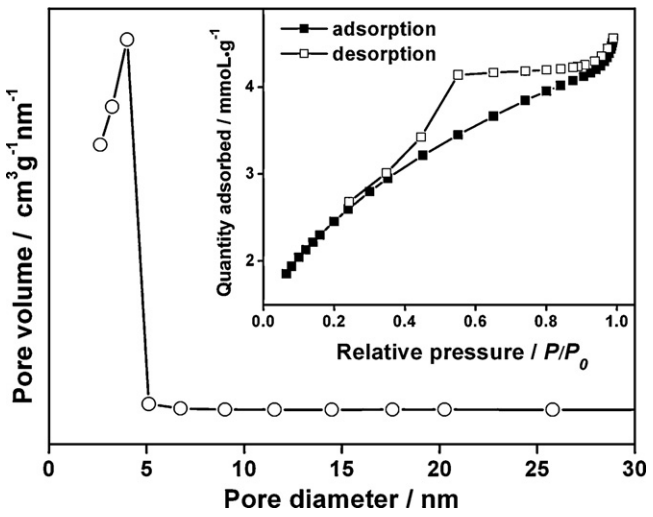

Fig. 3. Pore diameter distribution of $SnIn_4S_8$ microspheres. Inset shows the corresponding nitrogen adsorption–desorption isotherm.

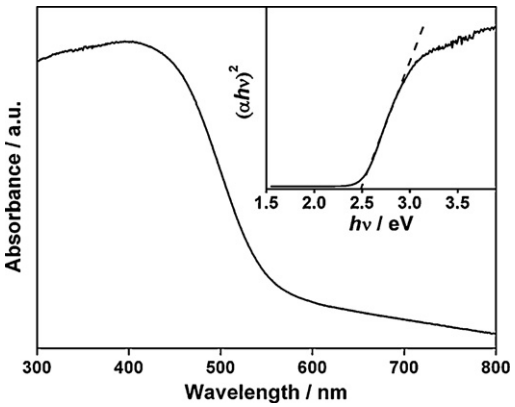

Fig. 4. UV–vis diffuse reflectance spectrum of the porous $SnIn_4S_8$ microspheres. Inset is the $(\alpha h\nu)^2$ against $h\nu$ curve.

$h\nu$ based on the direct transition is shown in inset of Fig. 4. The extrapolated value (the straight line to the *X*-axis) of $h\nu$ at $\alpha = 0$ gave an absorption edge energy at $E_g = 2.5$ eV. Taking into account the high surface-to-volume ratio, the ability to absorb visible light makes this hierarchically porous $SnIn_4S_8$ microsphere an effective photocatalyst for solar-driven applications.

3.2. Photocatalytic activity

Degradation of aqueous azo-dye (MO) was initially examined as a model reaction to evaluate the photocatalytic activity of the porous $SnIn_4S_8$ microspheres under visible light illumination ($\lambda > 400$ nm). For comparison, the MO degradations by binary sulfides In_2S_3 and SnS_2 and ternary chalcogenide $ZnIn_2S_4$ photocatalysts were also examined. Prior to irradiation, the adsorption property of $SnIn_4S_8$ towards MO was initially studied. From the result in Fig. 5, approximately 30% of MO was absorbed by $SnIn_4S_8$ in the dark for 1 h, which is about 3 times of that for In_2S_3 and SnS_2 and nearly 6 times of that for $ZnIn_2S_4$. The adsorption capability has a significant effect on the degradation behavior of organic pollutants, so $SnIn_4S_8$ is expected to exhibit a high photocatalytic degradation ability towards the target contaminant.

Blank experiment in the absence of the photocatalyst under visible light irradiation shows that the photolysis of MO was negligible.

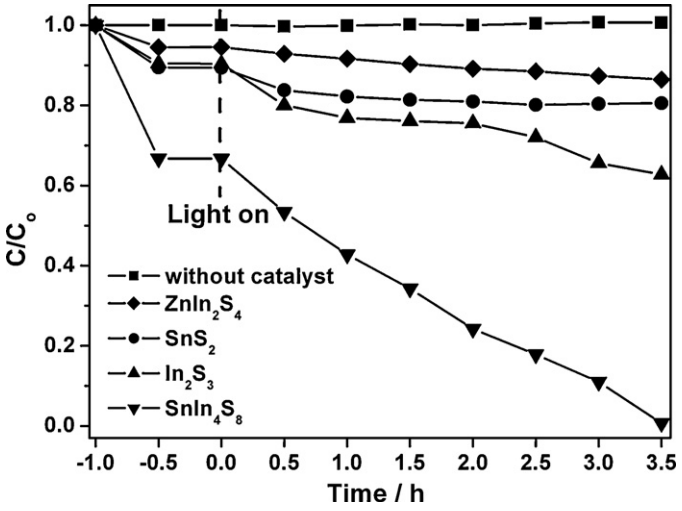

Fig. 5. Temporal concentration changes of MO as monitored by UV–vis absorption at 464 nm on porous $SnIn_4S_8$ microspheres under visible light irradiation. For comparison, the relevant data for possible binary constituent sulfides SnS_2 and In_2S_3 or the ternary chalcogenide $ZnIn_2S_4$ photocatalyst were also given.

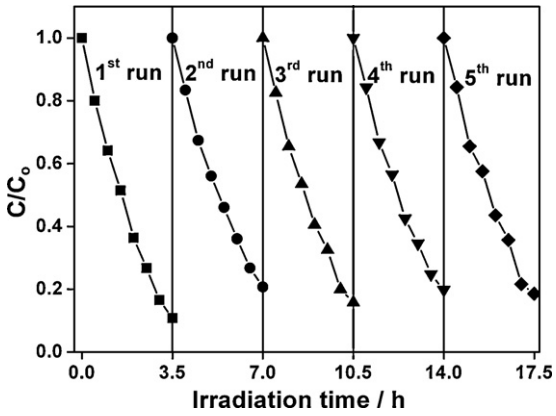

Fig. 6. Cycling runs for MO degradation in the presence of porous $SnIn_4S_8$ microspheres under visible light irradiation. The initial concentrations and volumes of MO aqueous solution were kept at 10 ppm and 80 mL for each run, respectively.

Nevertheless, when $SnIn_4S_8$ was added into the MO solution, the characteristic peak of MO at 464 nm decreased quickly under visible light irradiation (Fig. S1). After 3.5 h photoreaction, nearly 95% of MO was decolorized, showing an excellent photocatalytic activity of the as-prepared $SnIn_4S_8$ microsphere. On the contrary, the degradation rates of MO over In_2S_3, SnS_2 and $ZnIn_2S_4$ under the same irradiation condition were much lower. Only about 30%, 20%, and 12% of MO were degraded by In_2S_3, SnS_2, and $ZnIn_2S_4$, respectively (Fig. S4 and Fig. 5), which indicated that the porous $SnIn_4S_8$ microspheres possessed the highest photocatalytic activity.

It is well known that the application of a photocatalyst depends on both its efficiency and stability. However, it is previously reported that binary sulfides CdS and ZnS usually have poor photocatalytic stabilities [31]. Therefore, the stability of the porous $SnIn_4S_8$ microsphere photocatalyst has to be examined. For this purpose, $SnIn_4S_8$ was recycled after bleaching the MO under visible light irradiation and was reused five times in the degradation of MO to examine the chemical stability. It is surprisingly that $SnIn_4S_8$ microspheres did not show any apparent decrease in the photocatalytic activity towards MO decomposition even after five successive operations under visible light irradiation (Fig. 6). Both XRD and XPS examinations on $SnIn_4S_8$ (Figs. S5 and S6) further confirm that there were no obvious changes in the crystal structure or in the surfaces of the catalysts before and after photoreaction. All these results demonstrate that $SnIn_4S_8$ microspheres were highly stable.

In view of the excellent photocatalytic performance of porous $SnIn_4S_8$ microspheres towards MO degradation in aqueous solution, we extended the application of this new photocatalyst to remove other dyes from polluted water. RhB and MB are two common dyes, extensively used in various industrial applications. Fig. 7 displays the visible light induced photocatalytic activity for the degradation of RhB and MB over $SnIn_4S_8$ microspheres. The relevant data over In_2S_3 and SnS_2 under the same irradiation condition are also given in Fig. 7. It should be noted that RhB and MB are the known photosensitive dyes and could be decomposed under direct illumination even without photocatalyst [47,48], most likely due to the thermal effect caused by light source used. In this work, the thermal effect was excluded by cooling the reaction system to room temperature during the photocatalytic reactions. RhB and MB are relatively stable in aqueous solution under visible light irradiation as expected (Fig. 7). Similar to the MO result, $SnIn_4S_8$ also exhibited the strongest adsorption capability for RhB and MB among these three catalysts in dark. With the light irradiation for 4.5 h, RhB solution was almost colorless in the presence of $SnIn_4S_8$, while only 40% of RhB was decolorized by In_2S_3 and no obvious change of RhB in case of SnS_2 (Fig. 7a). It is also noted that the absorbance

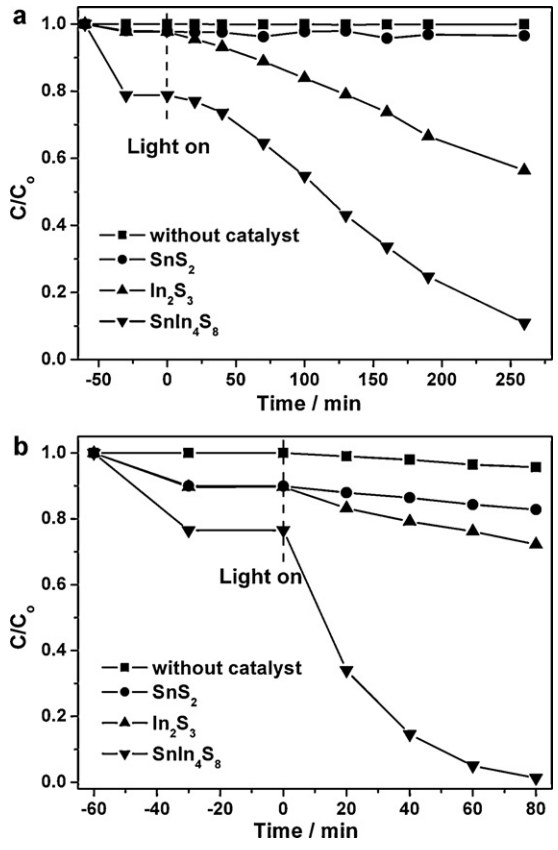

Fig. 7. Temporal concentration changes of (a) RhB (λ = 554 nm) and (b) MB (λ = 664 nm) on porous $SnIn_4S_8$ microspheres under visible light irradiation. For comparison, the relevant data for binary constituent sulfides SnS_2 and In_2S_3 were also given.

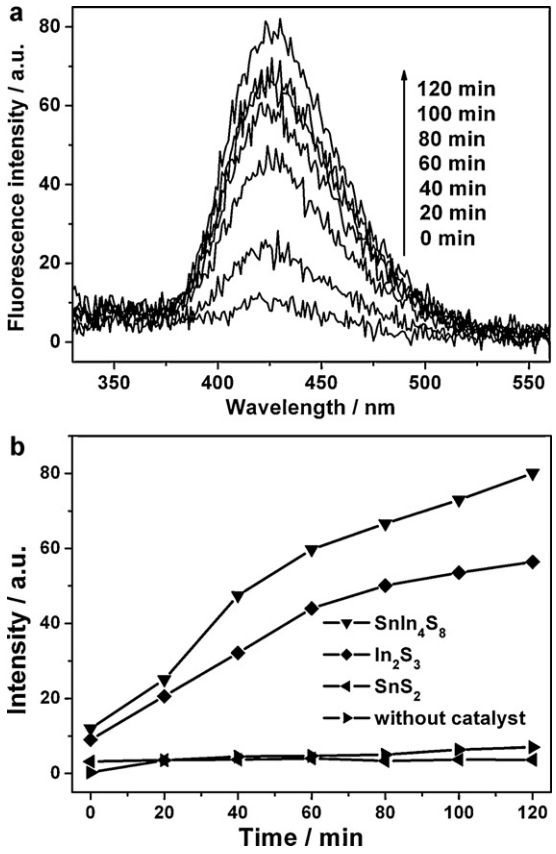

Fig. 8. (a) $^{\bullet}OH^{-}$ trapping photoluminescence spectra of porous $SnIn_4S_8$ microspheres under visible light irradiation in a solution of terephthalic acid at room temperature, when excited (Ex) at 312 nm, (b) plots of the induced fluorescence intensity (426 nm) against light irradiation time over porous $SnIn_4S_8$ microspheres. For comparison, the relevant data for binary constituent sulfides SnS_2 and In_2S_3 were also given.

maximum for RhB exhibited a significant blue shift from λ = 554 to 527 nm during the irradiation in the presence of $SnIn_4S_8$ (Fig. S7), which is due to the N-deethylation preferentially occurred in the photocatalytic process [49,50]. Besides, $SnIn_4S_8$ also showed degradation efficiency for MB much higher than those of In_2S_3 or SnS_2: after 80 min irradiation, MB solution decolorized completely in the presence of $SnIn_4S_8$ (Fig. 7b and Fig. S8). It is therefore reasonable that porous $SnIn_4S_8$ microsphere is a promising candidate for wastewater treatment in solar-driven applications.

Decolorization cannot mean the mineralization of the organic species. TOC, which reflects the general concentration of organics in solution, is used to evaluate the degree of degradation or mineralization of organic species. Table 1 summarizes the comparative results of TOC measurements before visible light irradiation and after 10 h irradiation. It can be seen that the mineralization yield of MO reached about 19% after 10 h irradiation, while that of RhB and MB is 100% after the same period of irradiation. This discrepancy in mineralization yield may be related to the structure of dyes and could thus be explained as follows: the molecular structure of MO is very stable with a special N=N double bond, which is hard to be broken or oxidized by visible light photocatalysis [51]. However, such a case can be totally changed for the conjugated systems and lateral chain in RhB or MB. As reviewed by Zhao et al. [52], two competitive pathways are involved in RhB degradation: N-deethylation and the cleavage of conjugated chromophore structure into small molecules, as reflected by the shift of the maximum absorption band and the changes in the absorption maximum of RhB.

Table 1
TOC results of the dyes over $SnIn_4S_8$ before and after visible light irradiation.

Dyes	TOC (mg L^{-1})		Mineralization rate for 5 h [%]
	Before irradiation	After10 h of irradiation	
MO	5.885	4.748	19
RhB	17.94	0	100
MB	9.068	0	100

The above characterization results show that porous $SnIn_4S_8$ microsphere is more active than binary constituent sulfides In_2S_3 and SnS_2 or ternary chalcogenide $ZnIn_2S_4$ as well for photocatalytic degradation of dyes under visible light irradiation. The excellent photocatalytic performance of porous $SnIn_4S_8$ microsphere may be related to several factors. The first important one might be the surface area. Numerous studies have verified that the surface area has a great influence on photocatalytic activity of semiconductors [12,13,32,53]. Since the present $SnIn_4S_8$ microsphere has an especially higher surface area (197 m^2 g^{-1}) than the other three samples (48 m^2 g^{-1} for In_2S_3, 32 m^2 g^{-1} for SnS_2, and 25 m^2 g^{-1} for $ZnIn_2S_4$), it can be expected that more reactants can be adsorbed on the surface of $SnIn_4S_8$ catalyst, leading to a higher photocatalytic efficiency [54,55]. Based on these, it is clear that the order of both adsorption capability and photocatalytic activity of these catalysts is in accordance with their corresponding surface areas. Therefore, large surface area of $SnIn_4S_8$ could be the dominant factor for the higher photocatalytic activity. In addition, well-defined porous configuration of $SnIn_4S_8$ microsphere relative to In_2S_3 and SnS_2 (Fig. S9) may also play an important role for its higher activity. This is because within such a hierarchically porous structure, irradi-

ation light will suffer successive reflection and scattering processes, which could enhance the light absorption and utilization efficiency (Scheme 1). Hydroxyl radicals (•OH) are commonly suggested as the primary oxidizing species in the photocatalytic oxidation processes. For samples $SnIn_4S_8$, In_2S_3, and SnS_2, the generation of •OH is confirmed by PL probe method in Fig. 8a, where the •OH trapping PL spectra of $SnIn_4S_8$ were shown in a terephthalic acid solution at room temperature under visible light irradiation. When $SnIn_4S_8$ system was irradiated by visible light, PL emission peak at 426 nm was found to gradually increase with prolonging the irradiation time. However, when $SnIn_4S_8$ system was in dark conditions, PL emission peak intensity was very weak and was almost unchanged regardless of the irradiation time (not shown). Thus, it is clear that the •OH was photogenerated on $SnIn_4S_8$ under visible light irradiation. Fig. 8b shows the plot of the induced PL intensity at 426 nm against irradiation time over different samples under visible light irradiation. It is observed that the PL intensity for $SnIn_4S_8$ was much stronger than that for In_2S_3 and SnS_2, which indicates the generation of large amount of •OH on $SnIn_4S_8$ system under the same conditions. This might be the third reason for the superior photocatalytic performance of $SnIn_4S_8$ over In_2S_3 and SnS_2.

4. Conclusion

We have demonstrated the synthesis of porous $SnIn_4S_8$ microspheres in a new tetragonal polymorph. These $SnIn_4S_8$ microspheres are highly photoactive and stable towards degradation of several typical organic dyes like MO, RhB, and MB in aqueous solutions under visible light irradiation. These findings are encouraging and will lead to the development of a new series of wastewater treatment photocatalysts. Further work will be highly necessary as to tune the porous microspheres for optimum oxidative ability and light absorption in efficient removal of persistent volatile organic pollutants such as aromatic hydrocarbons and polychlorinated biphenyls in air.

Acknowledgments

This work was financially supported by NSFC (No. 20773132, 20771101), National Basic Research Program of China (2009BAE89B01, 2009CB939801, 2007CB613301), Directional Program (KJCXZ-YW-M10), and FIPYT (No. 2008F3116).

Appendix A. Supplementary data

Supplementary data associated with this article can be found, in the online version, at doi:10.1016/j.jhazmat.2010.10.114.

References

[1] A. Panandikar, C. Fernandes, V.K.V. Rao, The cytotoxic properties malachite green are associated with increased demethylase, aryl hydrocarbon hydrolase and lipid peroxidation in primary cultures of syrian hamster embryo cells, Cancer Lett. 67 (1992) 93–101.
[2] A Panandikar, G.B. Maru, V.K.V. Rao, Dose–response effects of malachite green in free radical formation, lipid peroxidation and DNA damage in syrian hamster embryo cells and their modulation by antioxidants, Carcinogenesis 15 (1994) 2445–2448.
[3] C.R. Nony, M.C. Bowman, T. Cairns, Metabolism studies of an azo dye and pigment in the hamster based in analysis of the urine for potentially carcinogenic aromatic amine metabolites, J. Anal. Toxicol. 4 (1980) 132–140.
[4] R.B. Haveland-Smith, R.D. Combes, B.A. Briges, Studies on the genotoxicity of some fluorescein dyes, Mutat. Res. 88 (1981) 1–15.
[5] K. Inoue, M. Yoshida, M. Takahashi, H. Fujimoto, K. Ohnishi, K. Nakashima, M. Shibutani, M. Hirise, A. Nishikawa, A possible contribution of rubadin, a metabolite of madder color, to renal carcinogenesis in rats, Food Chem. Toxicol. 47 (2009) 752–759.
[6] F.C. Olak, N. Atar, A. Olgun, Biosorption of acidic dyes from aqueous solution by Paenibacillus macerans: kinetic, thermodynamic and equilibrium studies, Chem. Eng. J. 150 (2009) 122–130.
[7] G. Bayramoglu, B. Altintas, M.Y. Arica, Adsorption kinetics and thermodynamic parameters of cationic dyes from aqueous solutions by using a new strong cation-exchange resin, Chem. Eng. J. 152 (2009) 339–346.
[8] B. Merzouk, B. Gourich, A. Sekki, K. Madani, Ch. Vial, M. Barkaoui, Studies on the decolorization of textile dye wastewater by continuous electrocoagulation process, Chem. Eng. J. 149 (2009) 207–214.
[9] A.L. Ahmad, S.W. Puasa, Reactive dyes decolourization from an aqueous solution by combined coagulation/micellar-enhanced ultrafiltration process, Chem. Eng. J. 132 (2007) 257–265.
[10] L.C. Lei, Q.Z. Dai, M.H. Zhou, X.W. Zhang, Decolorization of cationic red X-GRL by wet-air oxidation: performance optimization and degradation mechanism, Chemosphere 68 (2007) 1135–1142.
[11] I.K. Konstantinou, T.A. Albanis, TiO_2-assisted photocatalytic degradation of azo dyes in aqueous solution: kinetic and mechanistic investigations – a review, Appl. Catal. B: Environ. 49 (2004) 1–14.
[12] D. Ravelli, D. Donde, M. Fagnoni, A. Albini, Photocatalysis. A multi-faceted concept for green chemistry, Chem. Soc. Rev. 38 (2009) 1999–2011.
[13] M.N. Chong, B. Jin, C.W.K. Chow, C. Saint, Recent developments in photocatalytic water treatment technology: a review, Water Res. 44 (2010) 2997–3027.
[14] M.R. Hoffmann, S.T. Martin, W.Y. Choi, D.W. Bahnemann, Environmental applications of semiconductor photocatalysis, Chem. Rev. 95 (1995) 69–96.
[15] M. Anpo, M. Takeuchi, The design and development of highly reactive titanium oxide photocatalysts operating under visible light irradiation, J. Catal. 216 (2003) 505–516.
[16] J.W. Tang, Z.G. Zou, J.H. Ye, Efficient photocatalytic decomposition of organic contaminants over $CaBi_2O_4$ under visible-light irradiation, Angew. Chem. Int. Ed. 43 (2004) 4463–4466.
[17] A. Fuerte, M.D. Hernández-Alonso, A.J. Maira, A. Martinez-Arias, M. Fernandez-Garcia, J.C. Coneasa, J. Soria, Visible light-activated nanosized doped-TiO_2 photocatalysts, Chem. Commun. (2001) 2718–2719.
[18] W. Zhao, C.C. Chen, X.Z. Li, J.C. Zhao, H. Hidaka, N. Serpone, Photodegradation of sulforhodamine-B dye in platinized titania dispersions under visible light irradiation: influence of platinum as a functional co-catalyst, J. Phys. Chem. B 106 (2002) 5022–5028.
[19] H. Kato, A. Kudo, Visible-light-response and photocatalytic activities of TiO_2 and $SrTiO_3$ photocatalysts codoped with antimony and chromium, J. Phys. Chem. B 106 (2002) 5029–5034.
[20] R. Asahi, T. Morikawa, T. Ohwaki, K. Aoki, Y. Taga, Visible-light photocatalysis in nitrogen-doped titanium oxides, Science 293 (2001) 269–271.
[21] M.H. Zhou, J.G. Yu, Preparation and enhanced daylight-induced photocatalytic activity of C, N, S-tridoped titanium dioxide powders, J. Hazard. Mater. 152 (2008) 1229–1236.
[22] N. Serpone, P. Maruthamuthu, P. Pichat, E. Pelizzetti, H. Hidaka, Exploiting the interparticle electron transfer process in the photocatalysed oxidation of phenol, 2-chlorophenol and pentachlorophenol: chemical evidence for electron and hole transfer between coupled semiconductors, J. Photochem. Photobiol. A 85 (1995) 247–255.
[23] Y. Bessekhouad, D. Robert, J.-V. Weber, Photocatalytic activity of Cu_2O/TiO_2, Bi_2O_3/TiO_2 and $ZnMn_2O_4/TiO_2$ heterojunctions, Catal. Today 101 (2005) 315–321.
[24] Y.J. Yan, X.Q. Qiu, H. Wang, L.P. Li, X.Z. Fu, L. Wu, G.S. Li, Synthesis of titanate/anatase composites with highly photocatalytic decolorization of dye under visible light irradiation, J. Alloy Compd. 460 (2008) 491–495.
[25] A. Kudo, K. Omori, H. Kato, A novel aqueous process for preparation of crystal form-controlled and highly crystalline $BiVO_4$ powder from layered vanadates at room temperature and its photocatalytic and photophysical properties, J. Am. Chem. Soc. 121 (1999) 11459–11467.
[26] G.S. Li, D.Q. Zhang, J.C. Yu, M.K.H. Leung, An efficient bismuth tungstate visible-light-driven photocatalyst for breaking down nitric oxide, Environ. Sci. Technol. 44 (2010) 4276–4281.
[27] J.W. Tang, Z.G. Zou, J.H. Ye, Effects of substituting Sr^{2+} and Ba^{2+} for Ca^{2+} on the structural properties and photocatalytic behaviors of $CaIn_2O_4$, Chem. Mater. 16 (2004) 1644–1649.
[28] D.W. Jing, L.J. Guo, A novel method for the preparation of a highly stable and active CdS photocatalyst with a special surface nanostructure, J. Phys. Chem. B 110 (2006) 11139–11145.
[29] H.B. Yin, Y. Wada, T. Kitamura, S. Yanagida, Photoreductive dehalogenation of halogenated benzene derivatives using ZnS or CdS nanocrystallites as photocatalysts, Environ. Sci. Technol. 35 (2001) 227–231.
[30] B.B. Kale, J.-O. Baeg, S.M. Lee, H. Chang, S.-J. Moon, C.W. Lee, $CdIn_2S_4$ nanotubes and "marigold" nanostructures: a visible-light photocatalyst, Adv. Funct. Mater. 16 (2006) 1349–1354.
[31] Z.B. Lei, W.S. You, M.Y. Liu, G.H. Zhou, T. Takata, M. Hara, K. Domen, C. Li, Photocatalytic water reduction under visible light on a novel $ZnIn_2S_4$ catalyst synthesized by hydrothermal method, Chem. Commun. (2003) 2142–2143.
[32] X.C. Wang, J.C. Yu, C.M. Ho, Y.D. Hou, X.Z. Fu, Photocatalytic activity of a hierarchically macro/mesoporous titania, Langmuir 21 (2005) 2552–2559.
[33] A. Hagfeldt, M. Grätzel, Light-induced redox reactions in nanocrystalline systems, Chem. Rev. 95 (1995) 49–68.
[34] J.H. Pan, H.Q. Dou, Z.G. Xiong, C. Xu, J.Z. Ma, X.S. Zhao, Porous photocatalysts for advanced water purifications, J. Mater. Chem. 20 (2010) 4512–4528.
[35] D.R. Rolison, Catalytic nanoarchitectures – the importance of nothing and the unimportance of periodicity, Science 299 (2003) 1698–1701.
[36] R. Dedryvère, P.E. Lippens, J.C. Jumas, I. Lefebvre-Devos, C. Pèrez Vicente, Influence of the sulfur vacancies on the electronic properties of $In_{16}Sn_4S_{32}$, Solid State Sci. 3 (2001) 267–274.

[37] T. Hirakawa, Y. Nosaka, Properties of $O_2^{\bullet-}$ and $OH^{\bullet}$ formed in TiO_2 aqueous suspensions by photocatalytic reaction and the influence of H_2O_2 and some ions, Langmuir 18 (2002) 3247–3254.
[38] D.Z. Li, Z.X. Chen, Y.L. Chen, W.J. Li, H.J. Huang, Y.H. He, X.Z. Fu, A new route for degradation of volatile organic compounds under visible light: using the bifunctional photocatalyst $Pt/TiO_{2-x}N_x$ in H_2–O_2 atmosphere, Environ. Sci. Technol. 42 (2008) 2130–2135.
[39] D. Larcher, G. Sudant, R. Patrice, J.M. Tarascon, Some insights on the use of polyols-based metal alkoxides powders as precursors for tailored metal-oxides particles, Chem. Mater. 15 (2003) 3543–3551.
[40] L.S. Zhong, J.S. Hu, A.M. Cao, Q. Liu, W.G. Song, L.J. Wan, 3D flowerlike ceria micro/nanocomposite structure and its application for water treatment and CO removal, Chem. Mater. 19 (2007) 1648–1655.
[41] D.V. Bavykin, V.N. Parmon, A.A. Lapkin, F.C. Walsh, The effect of hydrothermal conditions on the mesoporous structure of TiO_2 nanotubes, J. Mater. Chem. 14 (2004) 3370–3377.
[42] S.J. Gregg, K.S.W. Sing, Adsorption, Surface Area and Porosity, Academic Press, London, 1982.
[43] Y. Huang, Z.H. Ai, W.K. Ho, M.J. Chen, S.C. Lee, Ultrasonic spray pyrolysis synthesis of porous Bi_2WO_6 microspheres and their visible-light-induced photocatalytic removal of NO, J. Phys. Chem. C 114 (2010) 6342–6349.
[44] M. Muruganandham, Y. Kusumoto, Synthesis of N, C codoped hierarchical porous microsphere ZnS as a visible light-responsive photocatalyst, J. Phys. Chem. C 113 (2009) 16144–16150.
[45] C.W. Sun, J. Sun, G.L. Xiao, H.R. Zhang, X.P. Qiu, H. Li, L.Q. Chen, Mesoscale organization of nearly monodisperse flowerlike ceria microspheres, J. Phys. Chem. B 110 (2006) 13445–13452.
[46] S. Tsunekawa, T. Fukuda, A. Kasuya, Blue shift in ultraviolet absorption spectra of monodisperse CeO_{2-x} nanoparticles, J. Appl. Phys. 87 (2000) 1318–1322.
[47] K. Yu, S.G. Yang, H. He, C. Sun, C.G. Gu, Y.M. Ju, Visible light-driven photocatalytic degradation of rhodamine B over $NaBiO_3$: pathways and mechanism, J. Phys. Chem. A 113 (2009) 10024–10032.
[48] G.D. Yang, Z. Jiang, H.H. Shi, T.C. Xiao, Z.F. Yan, Preparation of highly visible-light active N-doped TiO_2 photocatalyst, J. Mater. Chem. 20 (2010) 5301–5309.
[49] Q. Wang, C.C. Chen, D. Zhao, W.H. Ma, J.C. Zhao, Change of adsorption modes of dyes on fluorinated TiO_2 and its effect on photocatalytic degradation of dyes under visible irradiation, Langmuir 24 (2008) 7338–7345.
[50] X. Hu, T. Mohamood, W. Ma, C. Chen, J.C. Zhao, Oxidative decomposition of rhodamine B dye in the presence of VO_2^+ and/or Pt(IV) under visible light irradiation: N-deethylation, chromophore cleavage, and mineralization, J. Phys. Chem. B 110 (2006) 26012–26018.
[51] M. Sun, D.Z. Li, W.J. Li, Y.B. Chen, Z.X. Chen, Y.H. He, X.Z. Fu, New photocatalyst, Sb_2S_3, for degradation of methyl orange under visible-light irradiation, J. Phys. Chem. C 112 (2008) 18076–18081.
[52] J.C. Zhao, C.C. Chen., W.H. Ma, Photocatalytic degradation of organic pollutants under visible light irradiation, Top. Catal. 35 (2005) 269–278.
[53] J.S. Hu, L.L. Ren, Y.G. Guo, H.P. Liang, A.M. Cao, L.J. Wan, C.L. Bai, Mass production and high photocatalytic activity of ZnS nanoporous nanoparticles, Angew. Chem. Int. Ed. 44 (2005) 1269–1273.
[54] T.J. Yan, J.L. Long, X.C. Shi, D.H. Wang, Z.H. Li, X.X. Wang, Efficient photocatalytic degradation of volatile organic compounds by porous indium hydroxide nanocrystals, Environ. Sci. Technol. 44 (2010) 1380–1385.
[55] L.P. Li, J.J. Liu, Y.G. Su, G.S. Li, X.B. Chen, X.Q. Qiu, T.J. Yan, Surface doping for photocatalytic purposes: relations between particle size, surface modifications, and photoactivity of SnO_2:Zn^{2+} nanocrystals, Nanotechnology 20 (2009) 155706–155715.